

Nonlinear Outcome of Gravitational Instability in Disks with Realistic Cooling

Bryan M. Johnson and Charles F. Gammie

Center for Theoretical Astrophysics, University of Illinois at Urbana-Champaign, 1110 West Green St., Urbana, IL 61801

ABSTRACT

We consider the nonlinear outcome of gravitational instability in optically-thick disks with a realistic cooling function. We use a numerical model that is local, razor-thin, and unmagnetized. External illumination is ignored. Cooling is calculated from a one-zone model using analytic fits to low temperature Rosseland mean opacities. The model has two parameters: the initial surface density Σ_0 and the rotation frequency Ω . We survey the parameter space and find: (1) The disk fragments when $\langle\langle\tau_c\rangle\rangle\Omega \sim 1$, where $\langle\langle\tau_c\rangle\rangle$ is an effective cooling time defined as the average internal energy of the model divided by the average cooling rate. This is consistent with earlier results that used a simplified cooling function. (2) The initial cooling time τ_{co} for a uniform disk with $Q = 1$ can differ by orders of magnitude from $\langle\langle\tau_c\rangle\rangle$ in the nonlinear outcome. The difference is caused by sharp variations in the opacity with temperature. The condition $\tau_{co}\Omega \sim 1$ therefore does not necessarily indicate where fragmentation will occur. (3) The largest difference between $\langle\langle\tau_c\rangle\rangle$ and τ_{co} is near the opacity gap, where dust is absent and hydrogen is largely molecular. (4) In the limit of strong illumination the disk is isothermal; we find that an isothermal version of our model fragments for $Q \lesssim 1.4$. Finally, we discuss some physical processes not included in our model, and find that most are likely to make disks more susceptible to fragmentation. We conclude that disks with $\langle\langle\tau_c\rangle\rangle\Omega \lesssim 1$ do not exist.

Subject headings: accretion, accretion disks, solar system: formation, galaxies: nuclei

1. Introduction

The outer regions of accretion disks in both active galactic nuclei (AGN) and young stellar objects (YSO) are close to gravitational instability (for a review see, for AGN: Shlosman

et al. 1990; YSOs: Adams & Lin 1993). Gravitational instability can be of central importance in disk evolution. In some disks, it leads to the efficient redistribution of mass and angular momentum (e.g. Larson 1984; Laughlin & Rozyczka 1996; Gammie 2001). In other disks, gravitational instability leads to fragmentation and the formation of bound objects. This may cause the truncation of circumnuclear disks (Goodman 2003), or the formation of planets (e.g. Boss 1997, and references therein).

We will restrict attention to disks whose potential is dominated by the central object, and whose rotation curve is therefore approximately Keplerian. Gravitational instability to axisymmetric perturbations sets in when the sound speed c_s , the rotation frequency Ω , and the surface density Σ satisfy

$$Q \equiv \frac{c_s \Omega}{\pi G \Sigma} < Q_{crit} \simeq 1 \quad (1)$$

(Toomre 1964; Goldreich & Lynden-Bell 1965). Here $Q_{crit} = 1$ for a “razor-thin” (two-dimensional) fluid disk model of the sort we will consider below, and $Q_{crit} = 0.676$ for a finite-thickness isothermal disk (Goldreich & Lynden-Bell 1965).¹ The instability condition (1) can be rewritten, for a disk with scale height $H \simeq c_s/\Omega$, around a central object of mass M_* ,

$$M_{disk} \gtrsim \frac{H}{r} M_*, \quad (2)$$

where $M_{disk} = \pi r^2 \Sigma$. For YSO disks $H/r \sim 0.1$ and thus a massive disk is required for instability. AGN disks are expected to be much thinner. The instability condition can be rewritten in a third, useful form if we assume that the disk is in a steady state and its evolution is controlled by internal (“viscous”) transport of angular momentum. Then the accretion rate $\dot{M} = 3\pi\alpha c_s^2 \Sigma/\Omega$, where $\alpha \lesssim 1$ is the usual dimensionless viscosity of Shakura & Sunyaev (1973), and

$$\dot{M} \gtrsim \frac{3\alpha c_s^3}{G} = 7.1 \times 10^{-4} \alpha \left(\frac{c_s}{1 \text{ km s}^{-1}} \right)^3 M_\odot \text{ yr}^{-1} \quad (3)$$

implies gravitational instability (e.g. Shlosman et al. (1990)). Disks dominated by external torques (e.g. a magnetohydrodynamic [MHD] wind) can have higher accretion rates (but not arbitrarily higher; see Goodman 2003) while avoiding gravitational instability.

For a young, solar-mass star accreting from a disk with $\alpha = 10^{-2}$ at $10^{-6} M_\odot \text{ yr}^{-1}$, equation (3) implies that instability occurs where the temperature drops below 17 K. Disks may not be this cold if the star is located in a warm molecular cloud where the ambient

¹For global models with radial structure, nonaxisymmetric instabilities typically set in for slightly larger values of Q (see Boss 1998 and references therein).

temperature is greater than 17 K, or if the disk is bathed in scattered infrared light from the central star (although there is some evidence for such low temperatures in the solar nebula, e.g. Owen et al. 1999). If the vertically-averaged value of α is small and internal dissipation is confined to surface layers, as in the layered accretion model of Gammie (1996), then instability can occur at higher temperatures, although equation (2) still requires that the disk be massive.

AGN disk heating is typically dominated by illumination from a central source. The temperature then depends on the shape of the disk. If the disk is flat or shadowed, however, and transport is dominated by internal torques, one can apply equation (3). For example, in the nucleus of NGC 4258 (Miyoshi et al. 1995) the accretion rate may be as large as $10^{-2} M_{\odot} \text{ yr}^{-1}$ (Lasota et al. 1996; Gammie et al. 1999). Equation (3) then implies that instability sets in where $T < 10^4(\alpha/10^{-2})$ K. If the disk is illumination-dominated then Q fluctuates with the luminosity of the central source.

In a previous paper (Gammie 2001), one of us investigated the effect of gravitational instability in cooling, gaseous disks in a local model. A simplified cooling function Λ was employed in these simulations, with a fixed cooling time τ_{co} :

$$\Lambda = -\frac{U}{\tau_{co}}, \quad (4)$$

where U is the internal energy per unit area. Disk fragmentation was observed for $\tau_{co}\Omega \lesssim 3$. The purpose of this paper is to investigate gravitational instability in a local model with more realistic cooling.

Several recent numerical experiments have included cooling, as opposed to isothermal or adiabatic evolution, and we can ask whether these results are consistent with Gammie (2001). Nelson et al. (2000) studied a global two-dimensional (thin) SPH model in which the vertical density and temperature structure is calculated self-consistently and each particle radiates as a blackbody at the surface of the disk. The initial conditions at a radius corresponding to the minimum initial value of Q (~ 1.5) for these simulations were $\Sigma_0 \approx 50 \text{ g cm}^{-2}$, $\Omega \approx 8 \times 10^{-10} \text{ s}^{-1}$; the initial cooling time under these circumstances is $\tau_{co} \approx 250 \Omega^{-1}$, so fragmentation is not expected and is not observed.

Durisen et al. (2001) consider a global three dimensional (3D) Eulerian hydrodynamics model in which the volumetric cooling rate varies with height above the midplane so as to preserve an isentropic vertical structure. The cooling time is fixed at each radius. Their cooling time $\gtrsim 10\Omega^{-1}$ at all radii, so fragmentation is not expected based on the criterion of Gammie (2001). The simulations show structure formation due to gravitational instabilities but not fragmentation.

Rice et al. (2003) consider a global 3D SPH model with a cooling time that is a fixed multiple of $\Omega^{-1}(r)$. They find that their disk fragments when $\tau_{co} \approx 3\Omega^{-1}$ and $M_{disk} = 0.1M_*$. For a more massive disk ($M_{disk} = 0.25M_*$), fragmentation occurred at somewhat higher cooling times ($\tau_{co} \approx 10\Omega^{-1}$). This is effectively a global generalization of the local model problem considered by Gammie (2001). The fact that the results are so consistent suggests that the local, thin approximation used in Gammie (2001) and here give a reasonable approximation to a global outcome.

Mayer et al. (2002) consider a global three dimensional SPH model of a circumstellar disk. Explicit cooling is not included, but the equation of state switches from isothermal to adiabatic when gravitational instability begins to set in. This is designed to account for the inefficient cooling of dense, optically thick regions. Fragmentation is observed. Realistic cooling can have a complex influence on disk evolution, and it is not clear that switching between isothermal and adiabatic behavior “brackets” the outcomes that might be obtained when full cooling is used.

Other notable recent work, such as that by Boss (2002), includes strong radiative heating in the sense that the effective temperature of the external radiation field T_{irr} is comparable to or larger than the disk midplane temperature T_c . In the limit that $T_{irr} \ll T_c$ we recover the limit considered here and in Gammie (2001); in the limit that $T_{irr} \gg T_c$ the disk is effectively isothermal.

The plan of this paper is as follows. In §2 we describe the model, with a detailed description of the cooling function given in §3. The results of numerical experiments are described in §4. Conclusions are given in §5.

2. Model

The model we use here is identical to that used in Gammie (2001) in every respect except that we use a more complicated cooling function. To make the description more self-contained, we summarize the basic equations of the model here. The model is local, in the sense that it considers a region of size L where $L/r_o \ll 1$ and r_o is a fiducial radius. We use a *local Cartesian* coordinate system $x \equiv r - r_o$ and $y \equiv (\phi - \Omega t)r_o$, where r, ϕ are the usual cylindrical coordinates and Ω is the orbital frequency at r_o . The model is also thin in the sense that matter is confined entirely to the plane of the disk.

Using the local approximation one can perform a formal expansion of the equations of motion in the small parameter L/r_o . The resulting equations of motion read, where \mathbf{v} is the velocity, P is the (two-dimensional) pressure, and ϕ is the gravitational potential with the

time-steady axisymmetric component removed:

$$\frac{D\mathbf{v}}{Dt} = -\frac{\nabla P}{\Sigma} - 2\Omega\hat{\mathbf{e}}_z \times \mathbf{v} + 3\Omega^2 x\hat{\mathbf{e}}_x - \nabla\phi. \quad (5)$$

For constant pressure and surface density, $\mathbf{v} = -\frac{3}{2}\Omega x\hat{\mathbf{e}}_y$ is an equilibrium solution to the equations of motion. This linear shear flow is the manifestation of differential rotation in the local model.

The equation of state is

$$P = (\gamma - 1)U, \quad (6)$$

where P is the two-dimensional pressure and U the two-dimensional internal energy. The two-dimensional (2D) adiabatic index γ can be mapped to a 3D adiabatic index Γ in the low-frequency (static) limit. For a non-self-gravitating disk $\gamma = (3\Gamma - 1)/(\Gamma + 1)$ (e.g. Goldreich, Goodman, & Narayan 1986; Ostriker, Shu, & Adams 1992). For a strongly self-gravitating disk, one can show that $\gamma = 3 - 2/\Gamma$. We adopt $\Gamma = 7/5$ throughout, which yields $\gamma = 11/7$.

The internal energy equation is

$$\frac{\partial U}{\partial t} + \nabla \cdot (U\mathbf{v}) = -P\nabla \cdot \mathbf{v} - \Lambda, \quad (7)$$

where $\Lambda = \Lambda(\Sigma, U, \Omega)$ is the cooling function, fully described below. Notice that there is no heating term; heating is due solely to shocks. Numerically, entropy is increased by artificial viscosity in shocks.

The gravitational potential is determined by the razor-thin disk Poisson equation:

$$\nabla^2\phi = 4\pi G\Sigma\delta(z). \quad (8)$$

For a single Fourier component of the surface density $\Sigma_{\mathbf{k}}$ this has the solution

$$\phi = -\frac{2\pi G}{|\mathbf{k}|}\Sigma_{\mathbf{k}}e^{i\mathbf{k}\cdot\mathbf{x}-|kz|}. \quad (9)$$

A finite-thickness disk has weaker self-gravity, but this does not qualitatively change the dynamics of the disk in linear theory (Goldreich & Lynden-Bell 1965).

We integrate the governing equations using a self-gravitating hydrodynamics code based on ZEUS (Stone & Norman 1992). ZEUS is a time-explicit, operator-split, finite-difference method on a staggered mesh. It uses an artificial viscosity to capture shocks. Our implementation has been tested on standard linear and nonlinear problems, such as sound waves and shock tubes. We use the “shearing box” boundary conditions, described in detail by Hawley et al. (1995), and solve the Poisson equation using the Fourier transform method,

modified for the shearing box boundary conditions. See Gammie (2001) for further details on boundary conditions, numerical methods and tests.

The numerical model is always integrated in a region of size $L \times L$ at a numerical resolution of $N \times N$. In linear theory the disk is most responsive at the critical wavelength $2c_s^2/G\Sigma_o$.² We have checked the dependence of the outcome on L and found that as long as $L \gtrsim 2c_s^2/G\Sigma_o$ the outcome does not depend on L . We have also checked the dependence of the outcome on N and found that the outcome is insensitive to N , at least for the models with $N \geq 256$ that we use.

3. Cooling Function

Our cooling function is determined from a one-zone model for the vertical structure of the disk. The disk cools at a rate per unit area

$$\Lambda \equiv 2\sigma T_e^4, \quad (10)$$

which defines the effective temperature T_e . The cooling function depends on the heat content of the disk and how that content is transported from the disk interior to the surface: by radiation, convection, or perhaps some more exotic form of turbulent transport such as MHD waves. Low temperature disks are expected to be convectively unstable (e.g. Cameron 1978; Lin & Papaloizou 1980). Cassen (1993) has argued, however, that the radiative heat flux in an adiabatically-stratified disk is comparable to the heat dissipated by turbulence (in an α -disk model), suggesting that convection is incapable of radically altering the vertical structure of the disk. We will consider only radiative transport.

If the disk is optically thick in the Rosseland mean sense, so that radiative transport can be treated in the diffusion approximation, then (Hubeny 1990)

$$T_e^4 = \frac{8}{3} \frac{T_c^4}{\tau} \quad (11)$$

where τ is the Rosseland mean optical depth and T_c is the central temperature. We will assume that $T_c \approx T$, where

$$T = \frac{\mu m_p c_s^2}{\gamma k_B}, \quad (12)$$

and

$$c_s^2 = \gamma(\gamma - 1) \frac{U}{\Sigma}, \quad (13)$$

²The wavelength corresponding to the minimum in the dispersion relation for axisymmetric waves.

which follows from the equation of state and the assumption that the radiation pressure is small (we have verified that this is never seriously violated). Here k_B is Boltzmann's constant, m_p is the proton mass, and μ is the mean mass per particle, which we have set to 2.4 in models with initial temperature below the boundary between the grain-evaporation opacity and molecular opacity and $\mu = 0.6$ in models with initial temperature above the boundary.

The optical depth is

$$\tau \equiv \int_0^\infty dz \kappa(\rho_z, T_z) \rho_z \quad (14)$$

where κ is the Rosseland mean opacity, ρ_z and T_z are local density and temperature, and z is the height above the midplane. Following the usual one-zone approximation,

$$\int_0^\infty dz \kappa(\rho_z, T_z) \rho_z \approx H \kappa(\bar{\rho}, \bar{T}) \bar{\rho} \quad (15)$$

where the overbar indicates a suitable average and $H \approx c_s(T)/\Omega$ is the disk scale height (we ignore the effects of self-gravity on the disk scale height, which is valid when locally $Q \gtrsim 1$). Taking $\bar{T} \approx T$ and $\bar{\rho} \approx \Sigma/(2H)$ then gives a final, closed expression for Λ .

We have adopted the analytic approximations to the opacities provided by Bell & Lin (1994). These opacities are dominated by, in order of increasing temperature: grains with ice mantles, grains without ice mantles, molecules, H^- scattering, bound-free/free-free absorption and electron scattering. The molecular opacity regime is commonly called the *opacity gap*; it is too hot for dust, but too cold for H^- scattering to contribute much opacity. The opacity can be as much as 4 orders of magnitude smaller than the $\sim 5 \text{ g cm}^{-2}$ typical of the dust-dominated opacity regime. It turns out that this feature plays a significant role in the evolution of gravitationally-unstable disks.

To sum up, the cooling function is

$$\Lambda(\Sigma, U, \Omega) = \frac{16}{3} \frac{\sigma T^4}{\tau}. \quad (16)$$

For a power-law opacity of the form $\kappa = \kappa_0 \rho^a T^b$, this implies that

$$\Lambda \sim \Sigma^{-5-3a/2+b} U^{4+a/2-b}. \quad (17)$$

From this it follows that the cooling time $\tau_c \equiv U/\Lambda$ scales as

$$\tau_c \sim \Sigma^{5+3a/2-b} U^{-3-a/2+b}. \quad (18)$$

If the disk evolves quasi-adiabatically (as it does if the cooling time is long compared to the dynamical time) then $U \sim \Sigma^\gamma$ and

$$\tau_c \sim \Sigma^{5-3\gamma+(a/2)(3-\gamma)+b(\gamma-1)}. \quad (19)$$

Table 1 gives a list of values for this scaling exponent for our nominal value of $\gamma = 11/7$. Notice that, when ice grains or metal grains are evaporating, and in the bound-free/free-free opacity regime, cooling time *decreases* as surface density *increases*.

Our cooling function is valid in the limit of large optical depth ($\tau \gg 1$). Since the disk becomes optically thin at some locations in the course of a typical run, we must modify this result so that the cooling rate does not diverge at small optical depth. A modification that produces the correct asymptotic behavior is

$$\Lambda = \frac{16}{3} \sigma T^4 \frac{\tau}{1 + \tau^2}. \quad (20)$$

This interpolates smoothly between the optically-thick and optically-thin regimes and is proportional to the (Rosseland mean) optical depth in the optically-thin limit. While it would be more physically sensible to use a Planck mean opacity in the optically-thin limit, usually the optically-thin regions contain little mass so their cooling is not energetically significant. An exception is in the opacity gap, where even high density regions become optically thin.

Our simulations begin with Σ and U constant. The velocity field is perturbed from the equilibrium solution to initiate the gravitational instability. The initial velocities are $v_x = \delta v_x$, $v_y = -\frac{3}{2}\Omega x + \delta v_y$, where $\delta \mathbf{v}$ is a Gaussian random field of amplitude $\langle \delta v^2 \rangle / c_s^2 = 0.1$. The power spectrum of perturbations is white noise ($v_k^2 \sim k^0$) in a band in wavenumber $k_{crit}/4 < |k| < 4k_{crit}$ surrounding the minimum $k_{crit} = 1/(\pi Q^2)$ (with $G = \Sigma_o = \Omega = 1$) in the density-wave dispersion relation. We have checked in particular cases that for $10^{-3} < \langle \delta v^2 \rangle / c_s^2 < 10$ the outcome is qualitatively unchanged. This is expected because disk perturbations (unlike cosmological perturbations) grow exponentially and the initial conditions are soon forgotten.

Excluding the initial velocity field, the initial conditions for a spatially-uniform disk consist of three parameters: Σ_o , U_o , and Ω . We fix $Q = 1$, leaving two degrees of freedom. In models with simple, scale-free cooling functions such as that considered by Gammie (2001), these degrees of freedom remain and can be scaled away by setting $G = \Sigma_o = \Omega = 1$. That is, there is a two-dimensional continuum of disks (with varying values of Σ_o and Ω , but the same value of Q) that are described by a single numerical model.

The opacity contains definite physical scales in density and temperature. The realistic cooling function considered here therefore removes our freedom to rescale the disk surface density and rotation frequency. That is, there is now a one-to-one correspondence between disks with fixed Σ and Ω and our numerical models.

The choice of Σ_o and Ω as labels for the parameter space is not unique. Internally in the

code we fix the initial volume density (in g cm^{-3}) and the initial temperature (in Kelvins). These choices are difficult to interpret, however, since they are tied to quantities that change over the course of the simulation; Ω and the mean value of Σ do not.

The cooling is integrated explicitly using a first-order scheme. The timestep is modified to satisfy the Courant condition and to be less than a fixed fraction of the shortest cooling time on the grid. We have varied this fraction and shown that the results are insensitive to it, provided that it is sufficiently small.

4. Nonlinear Outcome

4.1. Standard Run

Consider the evolution of a single “standard” run, with $\Sigma_o = 1.4 \times 10^5 \text{ g cm}^{-2}$ and $\Omega = 1.1 \times 10^{-7} \text{ sec}^{-1}$. This corresponds to $T_o = 1200$ and $\tau_{co} = 9.0 \times 10^4 \Omega^{-1}$. The model size is $L = 320G\Sigma_o/\Omega^2$ and numerical resolution 1024^2 . The model initially lies at the lower edge of the opacity gap.

The evolution of the kinetic, gravitational and thermal energy per unit area ($\langle E_k \rangle$, $\langle E_g \rangle$ and $\langle E_{th} \rangle$ respectively) normalized to $G^2\Sigma_o^3/\Omega^2$ ³ are shown in Figure 1. After the initial phase of gravitational instability the model settles into a statistically-steady, gravito-turbulent state. It does not fragment. Cooling is balanced by shock heating. Energy for driving the shocks is extracted from the shear flow, and the mean shear flow is enforced by the boundary conditions.

The turbulent state transports angular momentum outward via hydrodynamic and gravitational shear stresses. The dimensionless gravitational shear stress is

$$\alpha_{grav} = \frac{1}{\langle \frac{3}{2} \Sigma c_s^2 \rangle} \int_{-\infty}^{\infty} dz \frac{g_x g_y}{4\pi G} \quad (21)$$

where \mathbf{g} is the gravitational acceleration, and the dimensionless hydrodynamic shear stress is

$$\alpha_{hyd} = \frac{\Sigma v_x \delta v_y}{\langle \frac{3}{2} \Sigma c_s^2 \rangle} \quad (22)$$

where $\langle \rangle$ denote a spatial average. Figure 2 shows the evolution of $\langle \alpha_{grav} \rangle$ and $\langle \alpha_{hyd} \rangle$ in the standard run. Averaged over the last $230\Omega^{-1}$ of the run, $\langle \langle \alpha_{hyd} \rangle \rangle = 0.0079$, $\langle \langle \alpha_{grav} \rangle \rangle = 0.017$,

³The natural unit that can be formed from G , Σ and Ω .

and so the total dimensionless shear stress is $\langle\langle\alpha\rangle\rangle = 0.025$, where $\langle\langle\rangle\rangle$ denote a space and time average.

The mean stability parameter $\langle Q \rangle \equiv \langle c_s \rangle \Omega / \pi G \langle \Sigma \rangle$ averages 1.86 over the last $230\Omega^{-1}$ of the run. Because the temperature and surface density vary strongly, other methods of averaging Q will give different results.

Figure 3 shows a snapshot of the surface density at $t = 50\Omega^{-1}$. The structure is similar to that observed in Gammie (2001), with trailing density structures. The density structures are stretched into a trailing configuration by the prevailing shear flow. Their scale is determined by the disk temperature and surface density rather than the size of the box (see Gammie 2001).

4.2. Varying Σ_o and Ω

We now turn to exploring the two-dimensional parameter space of models. First consider a series of models with the same initial central temperature, but with varying τ_{co} . As τ_{co} is lowered the time-averaged gravitational potential energy per unit area $\langle\langle E_g \rangle\rangle$ increases monotonically in magnitude. The gravito-turbulent state becomes more extreme, with larger $\langle\langle\alpha\rangle\rangle$, larger perturbed velocities, and larger density contrasts. Eventually a threshold is crossed and the disk fragments.

Fragmentation is illustrated in Figure 4, which shows a snapshot from a run with $\Sigma_o = 6.6 \times 10^3 \text{ g cm}^{-2}$, $\Omega = 5.4 \times 10^{-9} \text{ sec}^{-1}$. This corresponds to $T_o = 1200$, $\tau_{co} = 0.025\Omega^{-1}$. The run has numerical resolution 256^2 and $L = 80G\Sigma_o/\Omega^2$. The largest bound object in the center of the figure was formed from the collision and coalescence of several smaller bound objects. A snapshot of the optical depth at the same point in the simulation is given in Figure 5. For each snapshot, red indicates high values of the mapped variable and blue indicates low values. Much of the disk is optically thick, but most of the low density regions are optically thin in the Rosseland mean sense.

Lowering τ_{co} sufficiently always leads to fragmentation. We have surveyed the parameter space of Ω and Σ_o to determine where the disk begins to fragment. Each model was run to $100\Omega^{-1}$.⁴ Figures 6 and 7 summarize the results. Two heavy solid lines are shown on each diagram. The upper line shows the most rapidly cooling simulations that show no signs of gravitational fragmentation (*nonfragmentation point*). Quantitatively, we define this as the point at which the time-averaged gravitational potential energy per unit area is equal

⁴In four cases we had to run the simulation longer to get converged results.

to $-3G^2\Sigma_o^3/\Omega^2$.⁵ The lower line shows the most slowly cooling simulations to show definite fragmentation (*fragmentation point*). Quantitatively, we define this as the point at which the gravitational potential energy per unit area is equal to $-300G^2\Sigma_o^3/\Omega^2$ *at some point during the run*.⁶ Figure 6 shows the data in the ρ_o, T_o plane, while Figure 7 shows the results in the Σ_o, Ω plane. The light contours are lines of constant τ_{co} .

The transition from persistent, gravito-turbulent outcomes to fragmentation is gradual and statistical in nature. Figure 8 shows the gravitational potential energy per unit area in the transition region for a series of runs with $T_o = 1200$ K. The abscissa is labeled with the initial cooling time $\tau_{co}\Omega$. There is a gradual, approximately logarithmic increase in the magnitude of $\langle\langle E_g \rangle\rangle$ as τ_{co} decreases. Runs in this region exhibit the transient formation of small bound objects, which might collapse if additional physics (e.g. the effects of MHD turbulence) were included in the model. Eventually $-\langle\langle E_g \rangle\rangle$ begins to increase dramatically, and we define the *transition point* as the beginning of this steep increase in gravitational binding energy.

Figure 9 shows the run of $\tau_{co}\Omega$ for the fragmentation point, transition point, and non-fragmentation point as a function of T_o . It is surprising that a disk can begin to exhibit signs of gravitational collapse for $\tau_{co}\Omega$ as large as 10^6 , and evade collapse for $\tau_{co}\Omega$ as small as 0.02. A naive application of the results of Gammie (2001) would suggest that fragmentation should occur for $\tau_{co}\Omega \lesssim 3$. Evidently this estimate can be off by orders of magnitude, with the largest error for $T_o \approx 10^3$ K, just below the opacity gap.

The physical argument for fragmentation at short cooling times is as follows (e.g. Shlosman et al. 1990). Thermal energy is supplied to the disk via shocks. Strong shocks occur when dense clumps collide with one another; this occurs on a dynamical timescale $\sim \Omega^{-1}$. If the disk cools itself more rapidly than shock heating cannot match cooling and fragmentation results. This argument is apparently contradicted by Figure 9. The resolution lies in finding an appropriate definition of cooling time. The disk loses thermal energy on the effective cooling timescale

$$\langle\langle \tau_c \rangle\rangle^{-1} \equiv \frac{\langle\langle \Lambda \rangle\rangle}{\langle\langle U \rangle\rangle}. \quad (23)$$

Figure 10 shows the run of $\langle\langle \tau_c \rangle\rangle$ at the fragmentation, transition, and non-fragmentation points. Evidently $\langle\langle \tau_c \rangle\rangle$ at transition lies between Ω^{-1} and $10\Omega^{-1}$. Figure 11 shows the run of τ_{co} and $\langle\langle \tau_c \rangle\rangle$ on the transition line. Just below the opacity gap they differ by as much as

⁵–3 is the potential energy per unit area of a wave at the critical wavelength in a $Q = 1$ disk with $\delta\Sigma/\Sigma = \sqrt{3}/\pi$. No bound objects are observed throughout the duration of these runs.

⁶These runs exhibit bound objects that persist for the duration of the run.

four orders of magnitude.

Why do τ_{co} and $\langle\langle\tau_c\rangle\rangle$ differ by such a large factor? The answer is related to the existence of sharp variations in opacity with temperature. Consider a disk near the lower edge of the opacity gap. Once gravitational instability sets in, fluctuations in temperature move parts of the disk into the opacity gap. There, the opacity is reduced by orders of magnitude. Since the cooling rate for an optically thick disk is proportional to κ^{-1} , the cooling time drops by a similar factor. Relatively small variations in temperature can thus produce large variations in cooling rate.

As in Gammie (2001), the result $\langle\langle\tau_c\rangle\rangle\Omega \gtrsim 1$ also implies a constraint on $\langle\langle\alpha\rangle\rangle$. Energy conservation implies that

$$\frac{3}{2}\Omega\langle\langle W_{xy}\rangle\rangle = \langle\langle\Lambda\rangle\rangle, \quad (24)$$

where W_{xy} is the total shear stress (hydrodynamic plus gravitational). Equivalently, stress by rate-of-strain is equal to the dissipation rate. Using the definition of $\langle\langle\tau_c\rangle\rangle$, this implies

$$\langle\langle\alpha\rangle\rangle = \left(\gamma(\gamma-1)\frac{9}{4}\Omega\langle\langle\tau_c\rangle\rangle\right)^{-1}. \quad (25)$$

Hence $\langle\langle\tau_c\rangle\rangle\Omega \gtrsim 1$ implies $\langle\langle\alpha\rangle\rangle \lesssim 1$. Figure 12 shows $\langle\langle\alpha\rangle\rangle$ vs $\langle\langle\tau_c\rangle\rangle$ for a large number of runs plotted against equation (25). For small values of $\langle\langle\tau_c\rangle\rangle$ the numerical values lie below the line. These models are not in equilibrium (i.e., not in a statistically-steady gravito-turbulent state), so the time average used in equation (24) is not well defined. For larger values of $\langle\langle\tau_c\rangle\rangle$ numerical results typically (there is noise in the measurement of both $\langle\langle\alpha\rangle\rangle$ and $\langle\langle\tau_c\rangle\rangle$ because the time average is taken over a finite time interval) lie slightly above the analytic result.

The bias toward points lying slightly above the line reflects the fact that $\langle\langle\alpha\rangle\rangle$ measures the rate of energy extraction from the shear while $\langle\langle\tau_c\rangle\rangle$ measures the rate at which that energy is transformed into thermal energy. If energy is lost, perhaps to numerical averaging at the grid scale, then more energy must be extracted from the shear flow to make up the difference. Overall, however, the agreement with the analytic result is good and demonstrates good energy conservation in the code.

The relationship between $\langle\langle\tau_c\rangle\rangle$ and $\langle\langle\alpha\rangle\rangle$ is interesting but not particularly useful because $\langle\langle\tau_c\rangle\rangle$ is no more readily calculated than $\langle\langle\alpha\rangle\rangle$; it depends on a complicated moment of the surface density and temperature. Only for constant cooling time have we been able to evaluate this moment analytically.

4.3. Isothermal Disks

We have assumed that external illumination of the disk is negligible. This approximation is valid when the effective temperature T_{irr} of the external irradiation is small compared to the central temperature of the disk. In the opposite limit, illumination controls the energetics of the disk and it is isothermal (if it is illuminated directly so that shadowing effects, such as those considered by Jang-Condell & Sasselov (2003) are negligible).

It is therefore worth studying the outcome of gravitational instability in an isothermal disk. The isothermal disk model has a single parameter: the initial value of Q . We ran models with varying values of Q and with $\langle \delta v^2 \rangle / c_s^2 = 0.1$. We find that models with $Q \lesssim 1.4$ fragment.

It is likely that the mass of the fragments, etc., depends on how an isothermal disk becomes unstable. Rapid fluctuation of the external radiation field is likely to produce a different outcome than dimming on a timescale long compared to the dynamical time.

5. Discussion

Using numerical experiments, we have identified those disks that are likely to fragment absent external heating. Disks with effective cooling times $\langle\langle\tau_c\rangle\rangle \lesssim \Omega^{-1}$ are susceptible to fragmentation. This is what one might expect based on the simple argument of Shlosman et al. (1990): if the disk cools more quickly than the self-gravitating condensations can collide with one another, then those collisions (which occur on a timescale $\sim \Omega^{-1}$) cannot reheat the disk and fragmentation is inevitable. But our results are at the same time surprising.

The effective cooling time depends on the nonlinear outcome of gravitational instability. It depends on the cooling function, which in turn depends sensitively on Σ and U . Since Σ and U vary strongly over the disk once gravitational instability has set in, it is difficult to estimate $\langle\langle\tau_c\rangle\rangle$ directly. One might be tempted to estimate $\langle\langle\tau_c\rangle\rangle(\Sigma, \Omega) \simeq \tau_{co}(\Sigma_o, \Omega, Q = 1)$, but our experiments show that this estimate can be off by as much as four orders of magnitude. The effect is particularly pronounced near sharp features in the opacity. For example, consider a model initially located just below the opacity gap with $\tau_{co}\Omega \gg 1$. Gravitational instability creates dense regions with higher temperatures, where dust is destroyed. The result is rather like having to shed one's blanket on a cold winter morning: the disk loses its thermal energy suddenly. Pressure support is lost and gravitational collapse ensues.

The difference between $\langle\langle\tau_c\rangle\rangle$ and $\tau_{co}(Q = 1)$ implies that a much larger region of the disk is susceptible to fragmentation than naive estimates based on the approximation $\langle\langle\tau_c\rangle\rangle \approx \tau_{co}$

might suggest. For example, consider an equilibrium disk model with $Q \gg 1$ at small r . As r increases, Q declines. Eventually $Q \sim 1$ and gravitational instability sets in. There is then a range of radii where $Q \sim 1$, $\langle\langle\tau_c\rangle\rangle\Omega \gtrsim 1$ and recurrent gravitational instability can transport angular momentum and prevent collapse. Generally speaking, however, the cooling time decreases with increasing radius. Eventually $\langle\langle\tau_c\rangle\rangle\Omega \sim 1$ and fragmentation cannot be avoided. By lowering our estimate of $\langle\langle\tau_c\rangle\rangle$, we narrow the range of radii over which recurrent gravitational instability can occur.

The general sense of our result is that it is extremely difficult to prevent a marginally-stable, $Q \sim 1$, optically-thick disk from fragmenting and forming planets (in circumstellar disks) or stars (in circumstellar and circumnuclear disks). This is particularly true for disks with $T \sim 10^3$ K, whose opacity is dominated by dust grains, i.e. disks whose temperature lies within a factor of several of the opacity gap.

Our numerical model uses a number of approximations. First, our treatment is razor-thin, i.e. all the matter is in a thin slice at $z = 0$. The effect of finite thickness on linear stability has been understood since Goldreich & Lynden-Bell (1965): it is stabilizing because gravitational attraction of neighboring columns of disk is diluted by finite thickness. The size of the effect may be judged by the fact that $Q = 0.676$ is required for marginal stability of a finite-thickness, isothermal disk.

The behavior of a finite-thickness disk in the nonlinear regime is more difficult to predict. Shocks will evidently deposit some of their energy away from the midplane, where it can be radiated away more quickly (because the energy is deposited at smaller optical depth - see Pickett et al. 2000). Radiative diffusion parallel to the disk plane (not included here) may enhance cooling of dense, hot regions. Both these effects are destabilizing. Ultimately, however, a numerical study is required. This is numerically expensive: one must resolve the disk vertically, on the scale height H , and horizontally, at the critical wavelength $2\pi QH$.

Second, we have ignored magnetic fields. While there may be astrophysical situations where cool disks have such low ionization that they are unmagnetized, most disks are likely to contain dynamically important magnetic fields that give rise to a dimensionless shear stress $\langle\langle\alpha\rangle\rangle \gtrsim 0.01$ (e.g. Hawley et al. 1995). These fields are likely to remove spin angular momentum from partially collapsed objects, destabilizing them. Numerical experiments including both gravitational fields and magnetohydrodynamics are necessarily three dimensional (the instability of Balbus & Hawley (1991) requires $\partial_z \neq 0$), and are thus numerically expensive.

Third, we have fixed γ and μ for the duration of each simulation. This eliminates the soft spots in the equation of state associated with ionization of atomic hydrogen and dissociation

of molecular hydrogen. In these locations the three dimensional γ dips below $4/3$, which is destabilizing.

Fourth, we have treated the physics of grain destruction and formation very simply. In using the Bell & Lin (1994) opacities we implicitly assume that grains reform in cooling gas on much less than a dynamical time. It is likely that grain re-formation will take some time (e.g. Hessman 1991) and this will further reduce the disk opacity and enhance fragmentation.

Fifth, we have neglected the effects of illumination. In the limit of strong external illumination, i.e. when the effective temperature of the irradiation T_{irr} is large compared to the disk central temperature T_c , the disk is isothermal (here T_c is the temperature of a dense condensation). We have carried out isothermal experiments and shown that, for initial velocity perturbations with $\langle \delta v^2 \rangle / c_s^2 = 0.1$, disks with $Q \lesssim 1.4$ fragment. Weaker illumination produces a more complicated situation that we have not explored here. Illumination-dominated disks that become unstable presumably do so because the external illumination declines, and the rate at which the external illumination changes may govern the nonlinear outcome.

We conclude that disks with $\langle \langle \tau_c \rangle \rangle \Omega \lesssim 1$ do not exist. Cooling in this case is so effective that fragmentation into condensed objects—stars, planets, or smaller accretion disks—is inevitable.

As an example application of this result, consider the model for the nucleus of NGC 1068 recently proposed by Lodato & Bertin (2003). Their model is an extended marginally-stable self-gravitating disk of the type investigated here and originally proposed by Goldreich & Lynden-Bell (1965) for galactic disks and Paczynski (1978) for accretion disks, although their disk is sufficiently massive that it modifies the rotation curve as well. Based on their Figure 3, at a typical radius of 0.5 pc, $\Sigma_o \simeq 10^4$ and $\Omega \simeq 10^{-9}$. According to our Figure 7 this disk is about 2 orders of magnitude too dense to avoid fragmentation. While it may be possible to avoid this conclusion by invoking strong external heating, the energy requirements are severe, as outlined in Goodman (2003). The disk proposed by Lodato & Bertin (2003) would therefore fragment into stars on a short timescale.

This work was supported by NSF grant AST 00-03091, PHY 02-05155, and NASA grant NAG 5-9180.

REFERENCES

Adams, F.C., & Lin, D.N.C. 1993, in *Protostars and Planets III* (Tucson: Arizona), 721

Balbus, S. A. & Hawley, J. F. 1991, *ApJ*, 376, 214

Bell, K.R. & Lin, D.N.C. 1994, *ApJ*, 427, 987

Boss, A. P. 1997, *Science*, 276, 1836

Boss, A. P. 1998, *ApJ*, 503, 923

Boss, A.P. 2002, *ApJ*, 576, 462

Cameron, A.G.W. 1978, *Moon & Planets*, 18, 5

Cassen, P. 1993, *Lunar and Planetary Institute Conference Abstracts*, 24, 261

H. Jang-Condell & D. D. Sasselov 2003, *ApJ*, submitted (astro-ph/0304330).

Durisen, R.H., Mejia, A.C., Pickett, B.K., & Hartquist, T.W. 2001, *ApJ*, 563, L157

Gammie, C.F. 1996, *ApJ*, 457, 355

Gammie, C.F. 2001, *ApJ*, 553, 174

Gammie, C.F., Narayan, R., & Blandford, R. 1999, *ApJ*, 516, 177

Goldreich, P., Goodman, J., & Narayan, R. 1986, *MNRAS*, 221, 339

Goldreich, P. & Lynden-Bell, D. 1965, *MNRAS*, 130, 125

Goodman, J. 2003, *MNRAS*, 339, 937

Hawley, J.F., Gammie, C.F., & Balbus, S.A. 1995, *ApJ*, 440, 742

Hessman, F.V. 1991, *A&A*, 246, 137

Hubeny, I. 1990, *ApJ*, 351, 632

Larson, R. B. 1984, *MNRAS*, 206, 197

Laughlin, G. & Rozyczka, M. 1996, *ApJ*, 456, 279

Lasota, J.-P., Abramowicz, M.A., Chen, X., Krolik, J., Narayan, R., & Yi, I. 1996, *ApJ*, 462, 142

Lin, D.N.C., & Papaloizou, J.C.B. 1980, MNRAS, 191, 37

Lodato, G. & Bertin, G. 2003, A&A, 398, 517

Mayer, L., Quinn, T., Wadsley, J., & Stadel, J. 2002, Science, 298, 1756

Miyoshi, M., Moran, J., Herrnstein, J., Greenhill, L., Nakai, N., Diamond, P., & Inoue, M. 1995, Nature, 373, 127

Nelson, A.F., Benz, W., & Ruzmaikina, T. 2000, ApJ, 529, 357

Ostriker, E. C., Shu, F. H., & Adams, F. C. 1992, ApJ, 399, 192

Owen, T., Mahaffy, P., Niemann, H.B., Atreya, S., Donahue, T., Bar-Nun, A., & de Pater, I. 1999, Nature, 402, 269

Paczynski, B. 1978, Acta Astronomica, 28, 91

Pickett, B.K., Cassen, P., Durisen, R.H., & Link, R. 2000, ApJ, 529, 1034

Rice, W.K.M., Armitage, P.J., Bate, M.R., & Bonnell, I.A. 2003, MNRAS, 339, 1025

Shakura, N.I., & Sunyaev, R.A. 1973, A&A, 24, 337

Shlosman, I., & Begelman, M., & Frank, J. 1990, Nature, 345, 679

Stone, J. M. & Norman, M. L. 1992, ApJS, 80, 753

Toomre, A. 1964, ApJ, 139, 1217

Table 1. Scaling Exponent for Cooling Time as a Function of Surface Density

Opacity Regime	a	b	Exponent
Ice grains	0	2	10/7
Evaporation of ice grains	0	-7	-26/7
Metal grains	0	1/2	4/7
Evaporation of metal grains	1	-24	-89/7
Molecules	2/3	3	52/21
H ⁻ scattering	1/3	10	131/21
Bound-free and free-free	1	-5/2	-3/7
Electron scattering	0	0	2/7

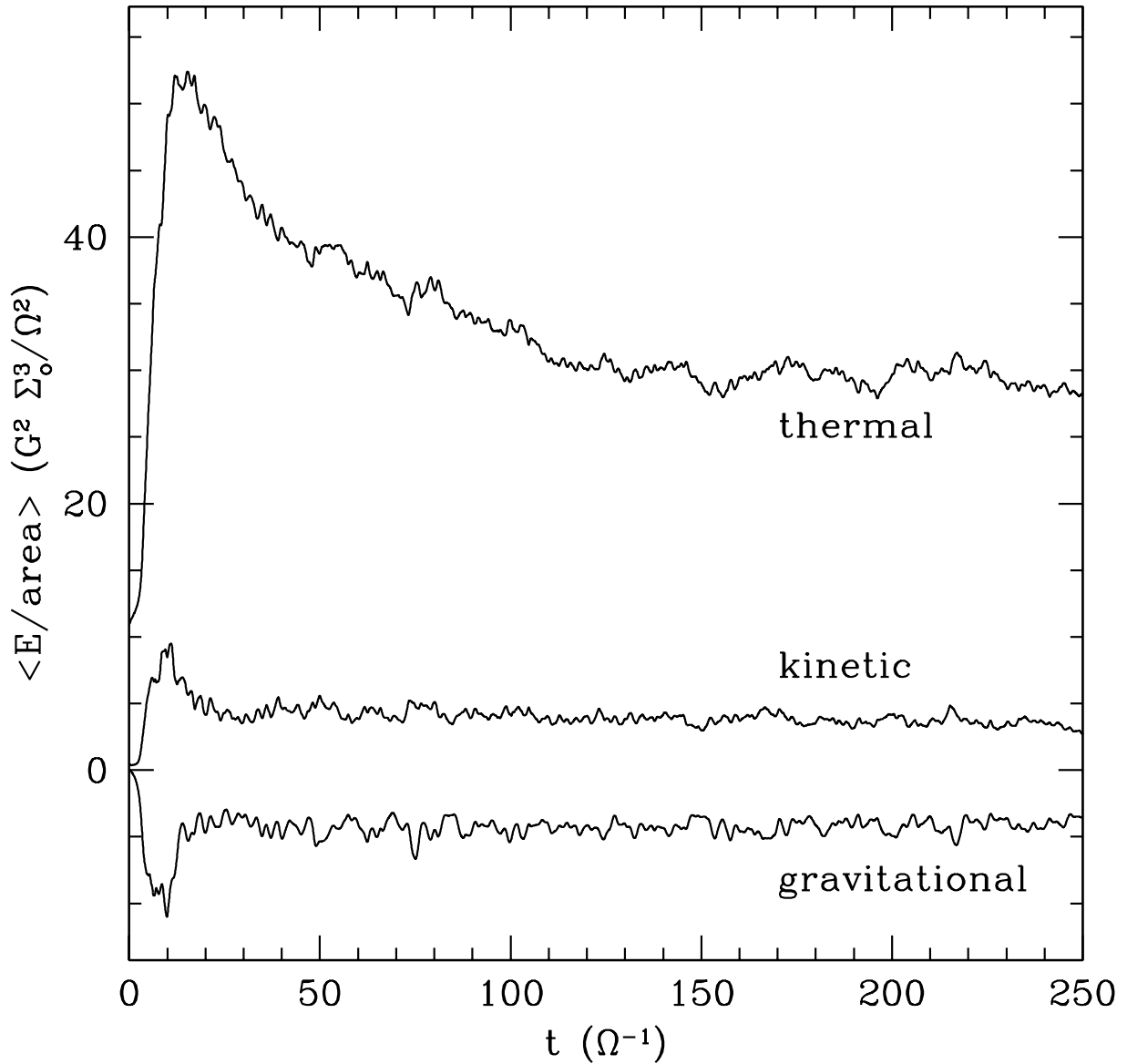


Fig. 1.— Evolution of the kinetic, gravitational, and thermal energy per unit area, normalized to $G^2 \Sigma_o^3 / \Omega^2$, in the standard run, which has $L = 320G\Sigma_o/\Omega^2$, resolution 1024^2 , and $\tau_{co} = 9.0 \times 10^4 \Omega^{-1}$.

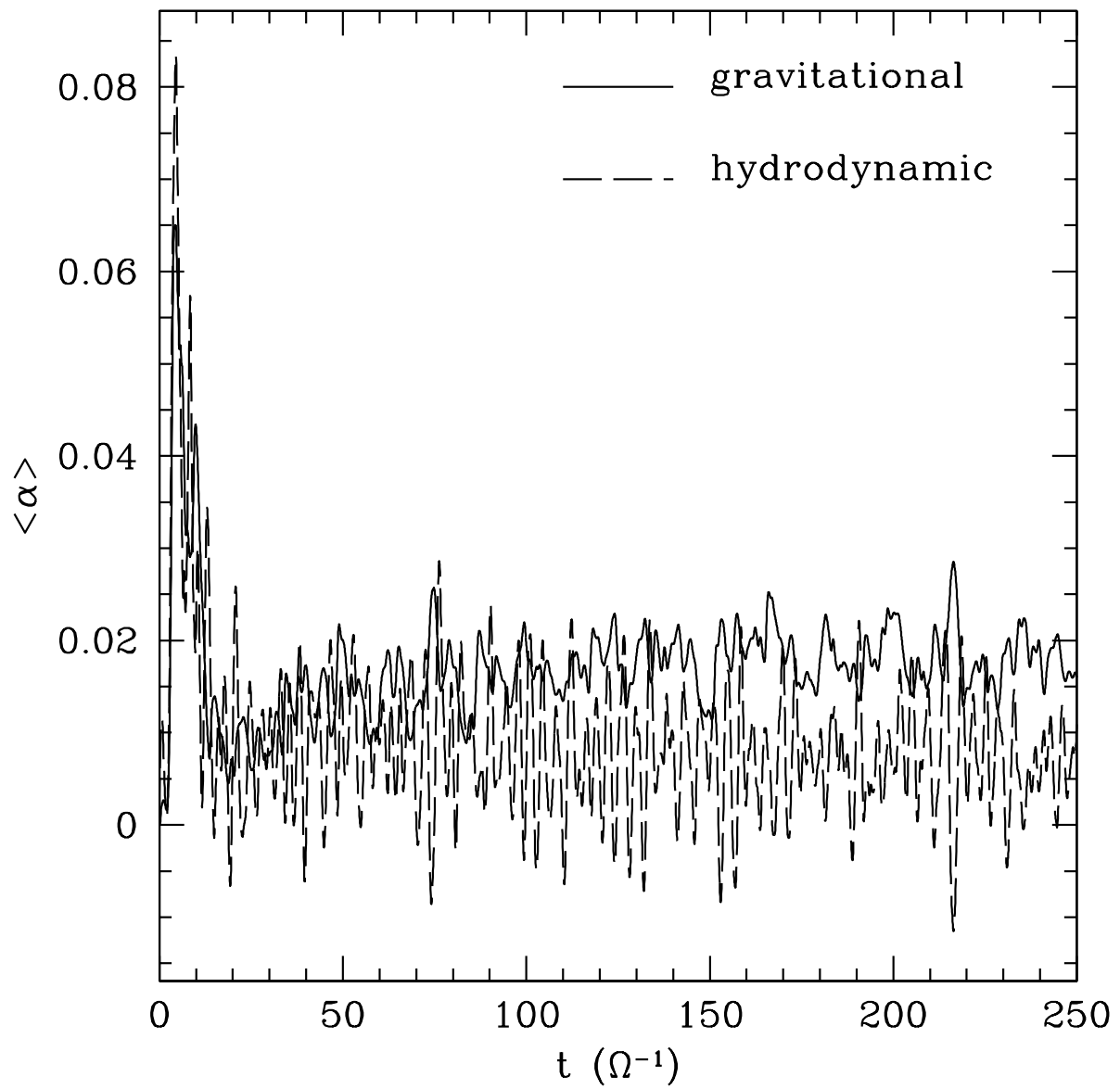


Fig. 2.— Evolution of the gravitational (solid line) and hydrodynamic (dashed line) pieces of $\langle \alpha \rangle$ in the standard run.

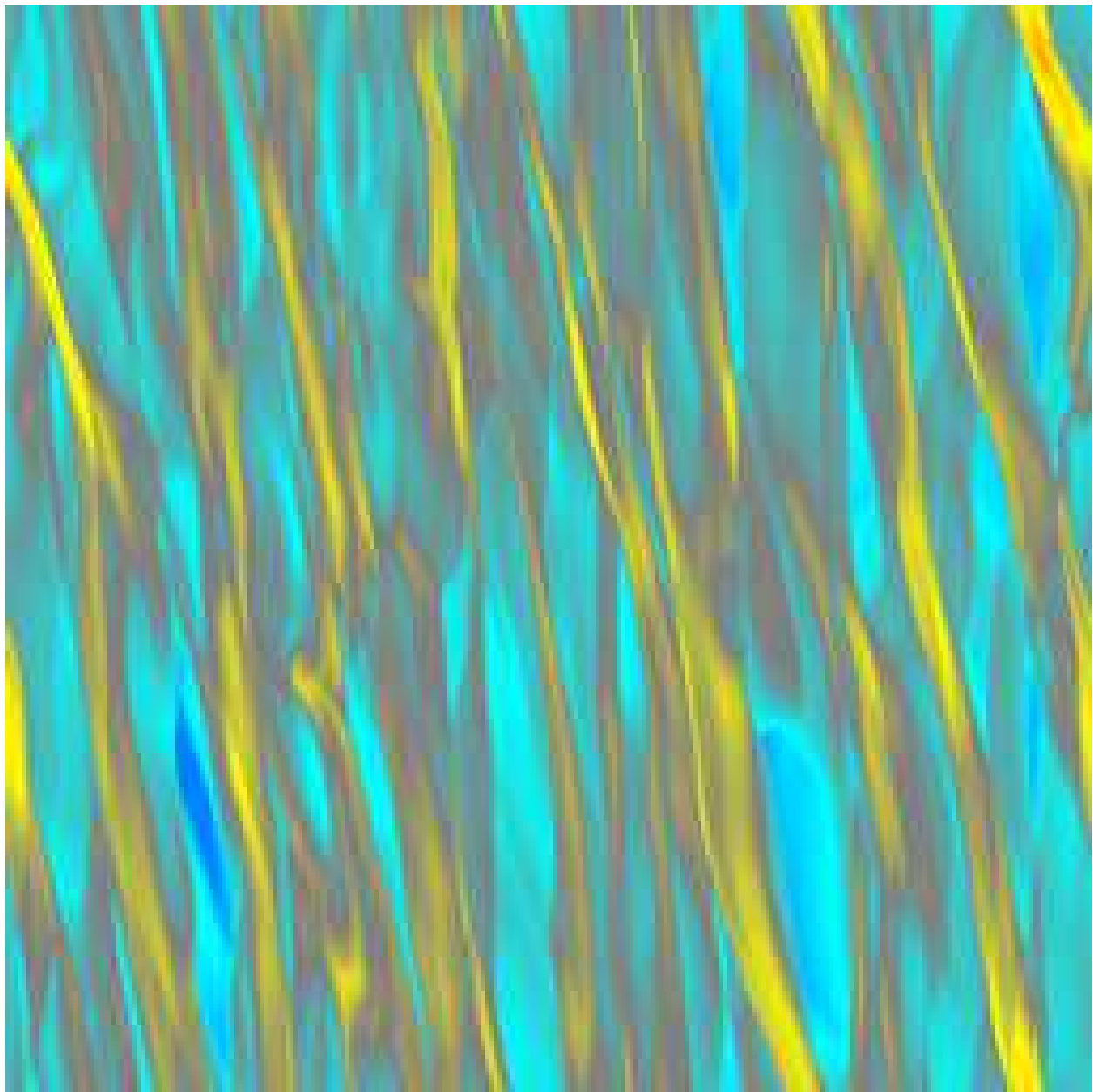


Fig. 3.— Map of surface density at $t = 50\Omega^{-1}$ in the standard run. Blue is low density ($0.2\Sigma_o$) and yellow is high density ($3\Sigma_o$).

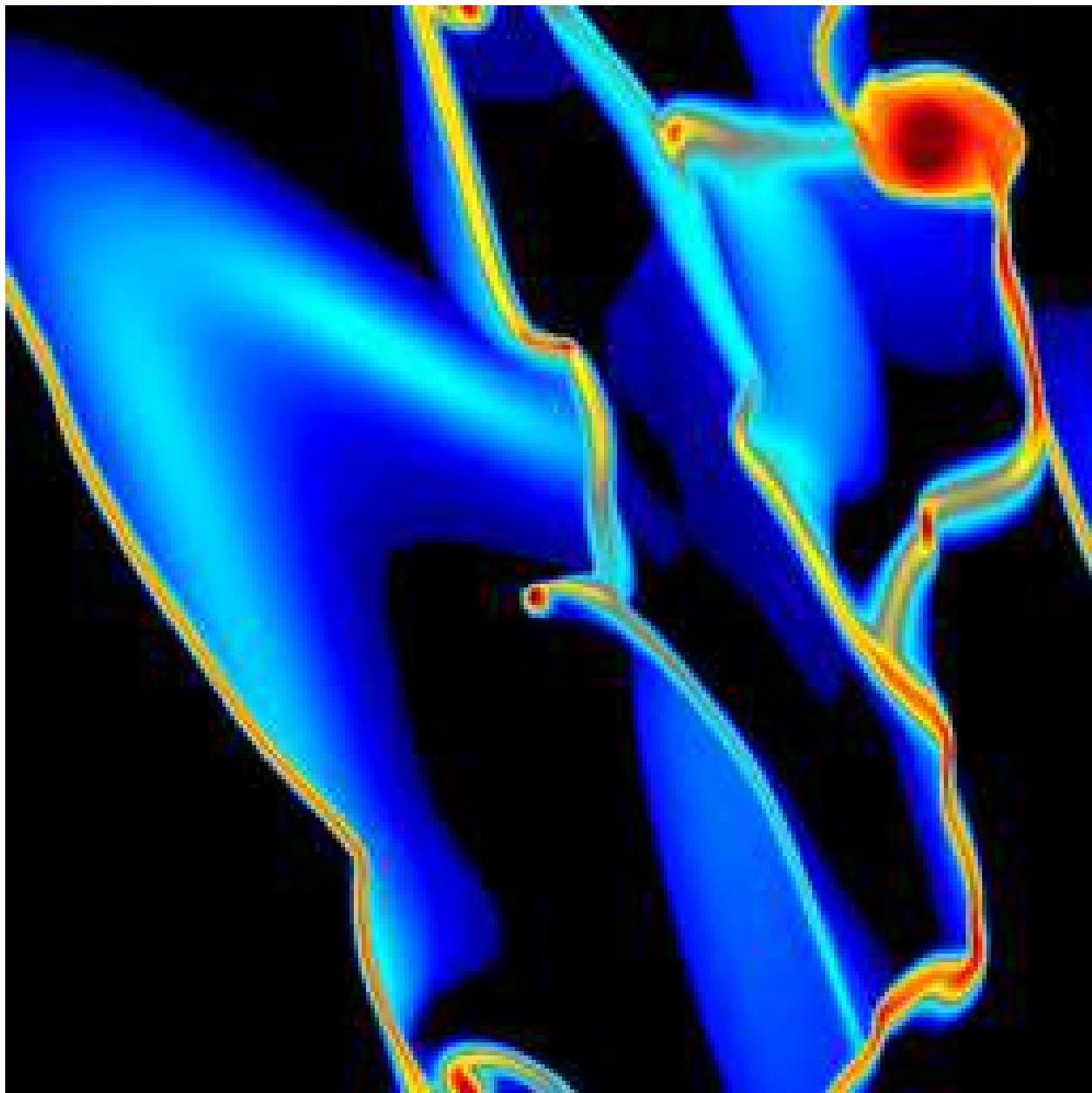


Fig. 4.— Map of surface density in a run with $\tau_{co} = 0.025\Omega^{-1}$. Black is low density ($10^{-2}\Sigma_o$) and red is high density ($10^2\Sigma_o$).

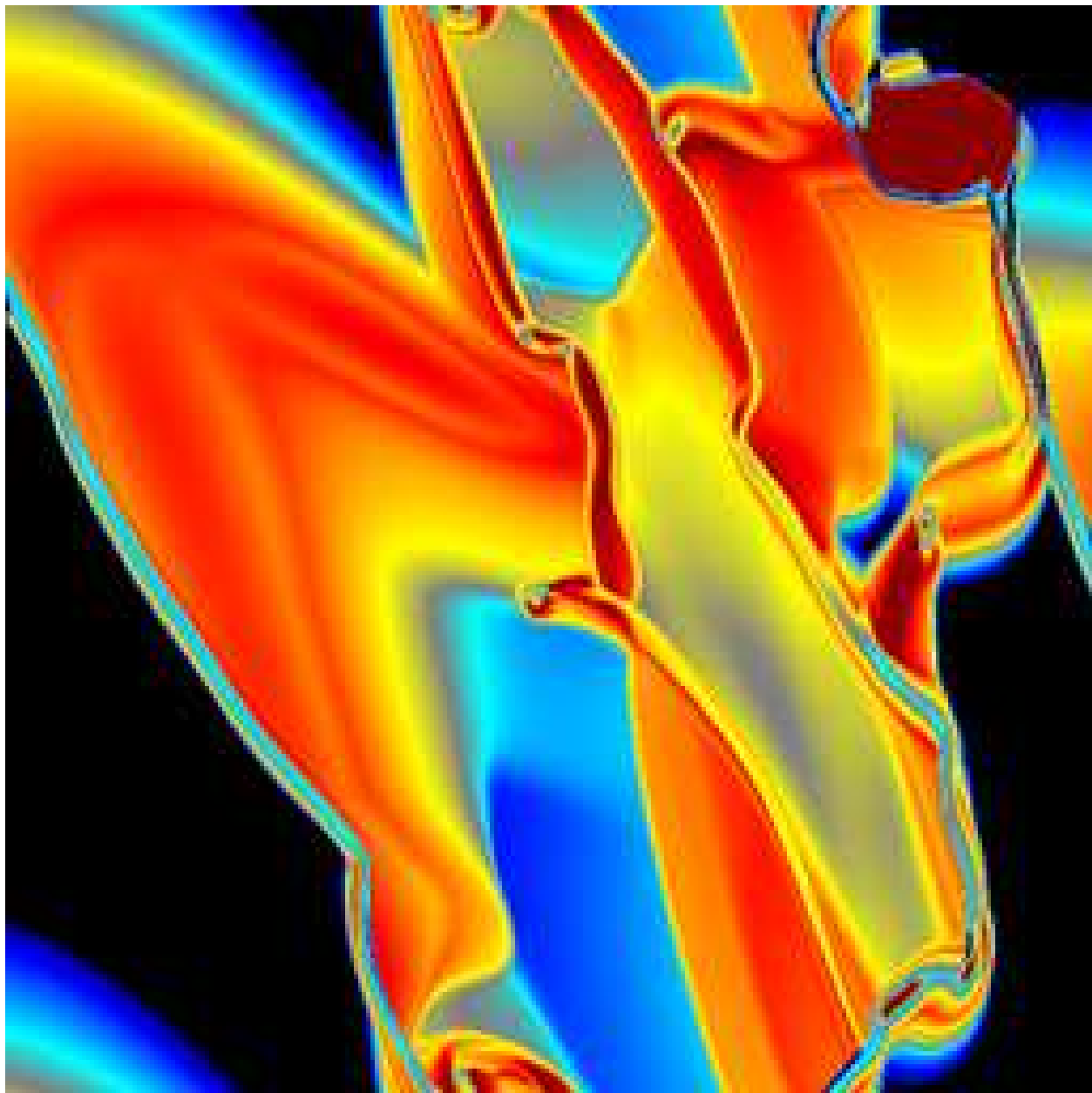


Fig. 5.— Map of optical depth in a run with $\tau_{eo} = 0.025\Omega^{-1}$. Black is low optical depth (10^{-2}) and red is high optical depth (10^4).

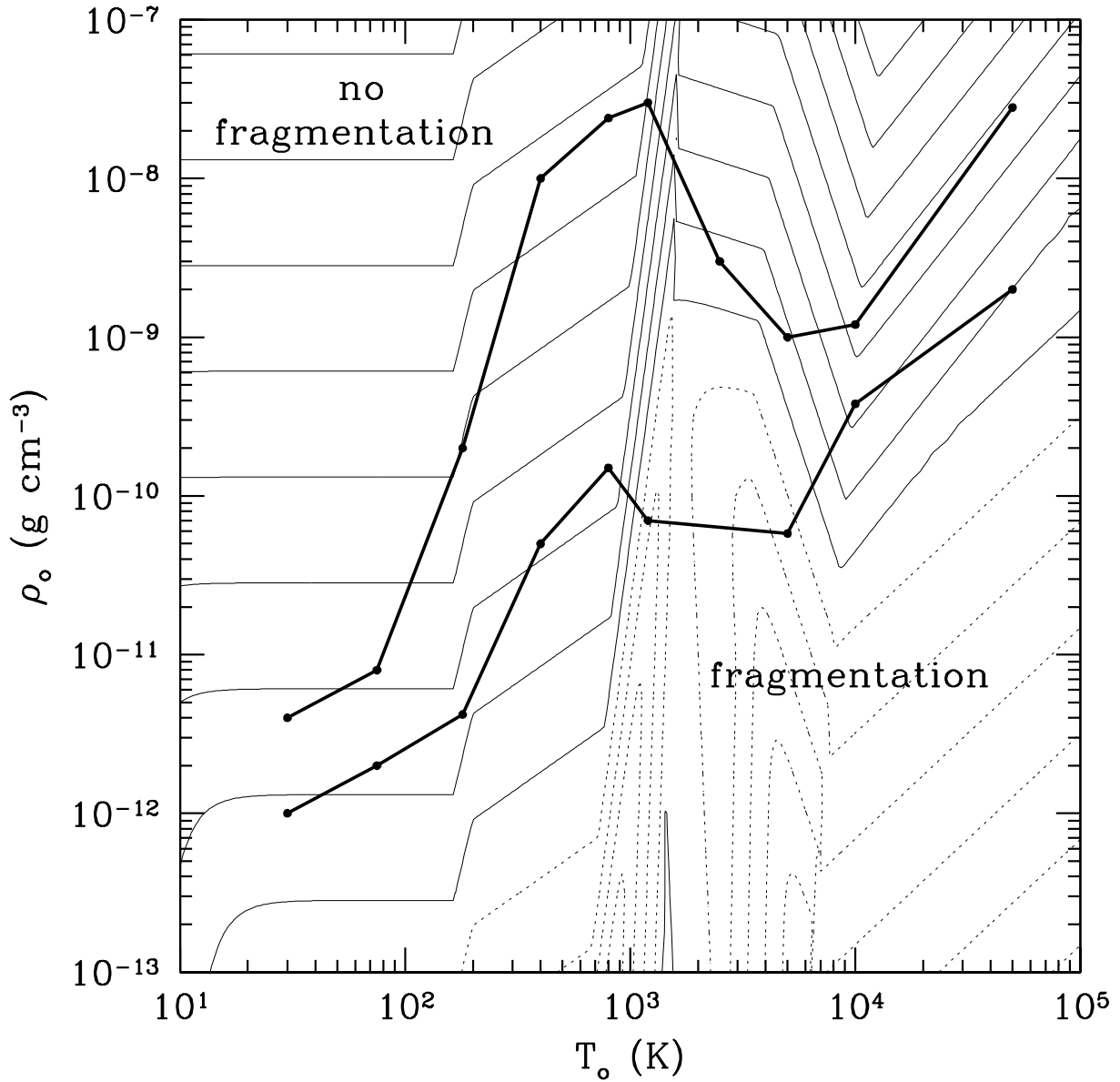


Fig. 6.— Location of the critical curves as a function of initial volume density and temperature (in cgs units). Each contour line is an order of magnitude change in τ_{co} , solid/dotted lines indicating positive/negative integer values of $\log(\tau_{co})$.

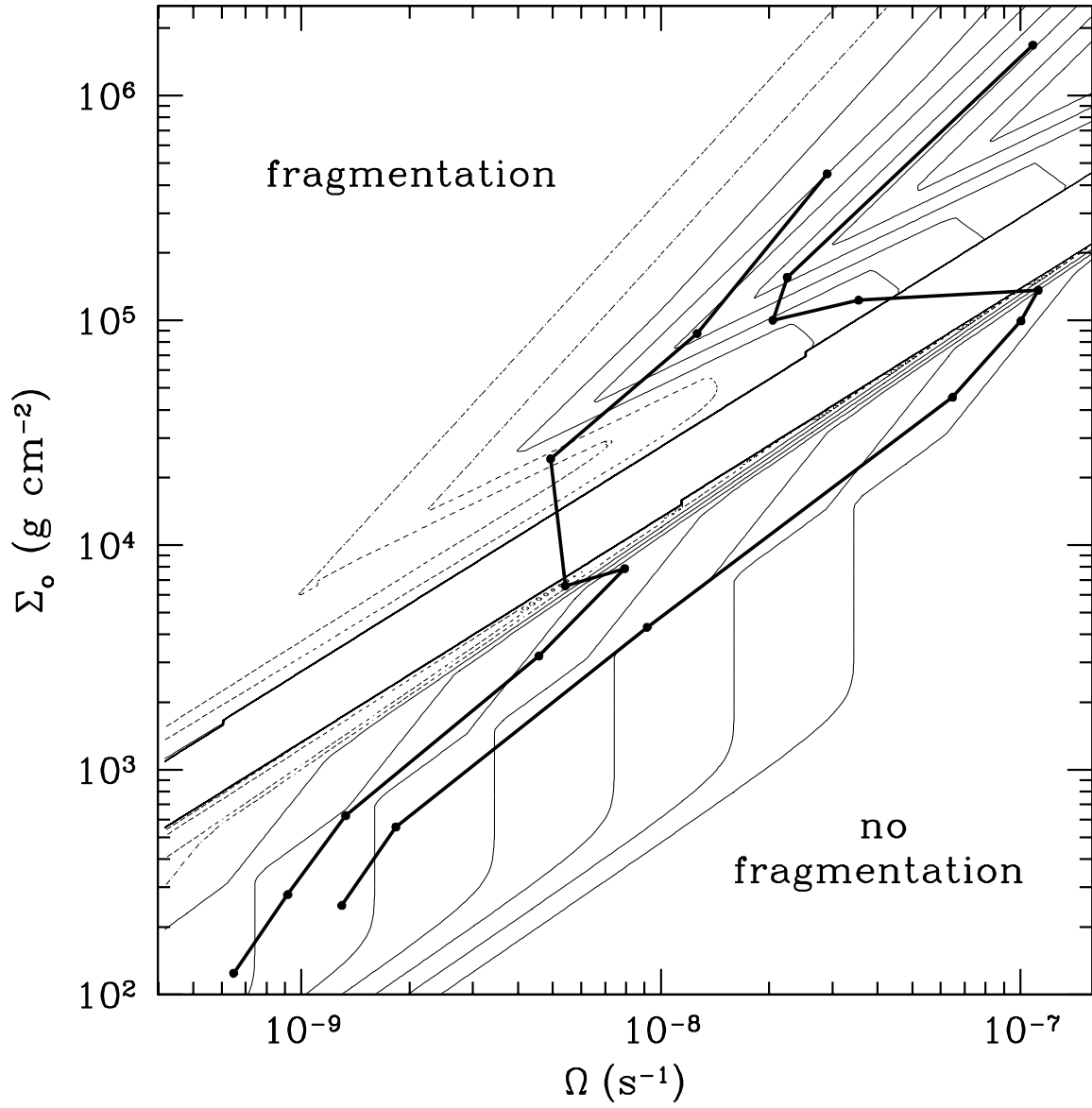


Fig. 7.— Location of the critical curves as a function of initial surface density and rotation frequency (in cgs units). Each contour line is an order of magnitude change in τ_{co} , solid/dotted lines indicating positive/negative integer values of $\log(\tau_{co})$. The gap in the center of the plot is due to the discontinuous jump in the value of μ .

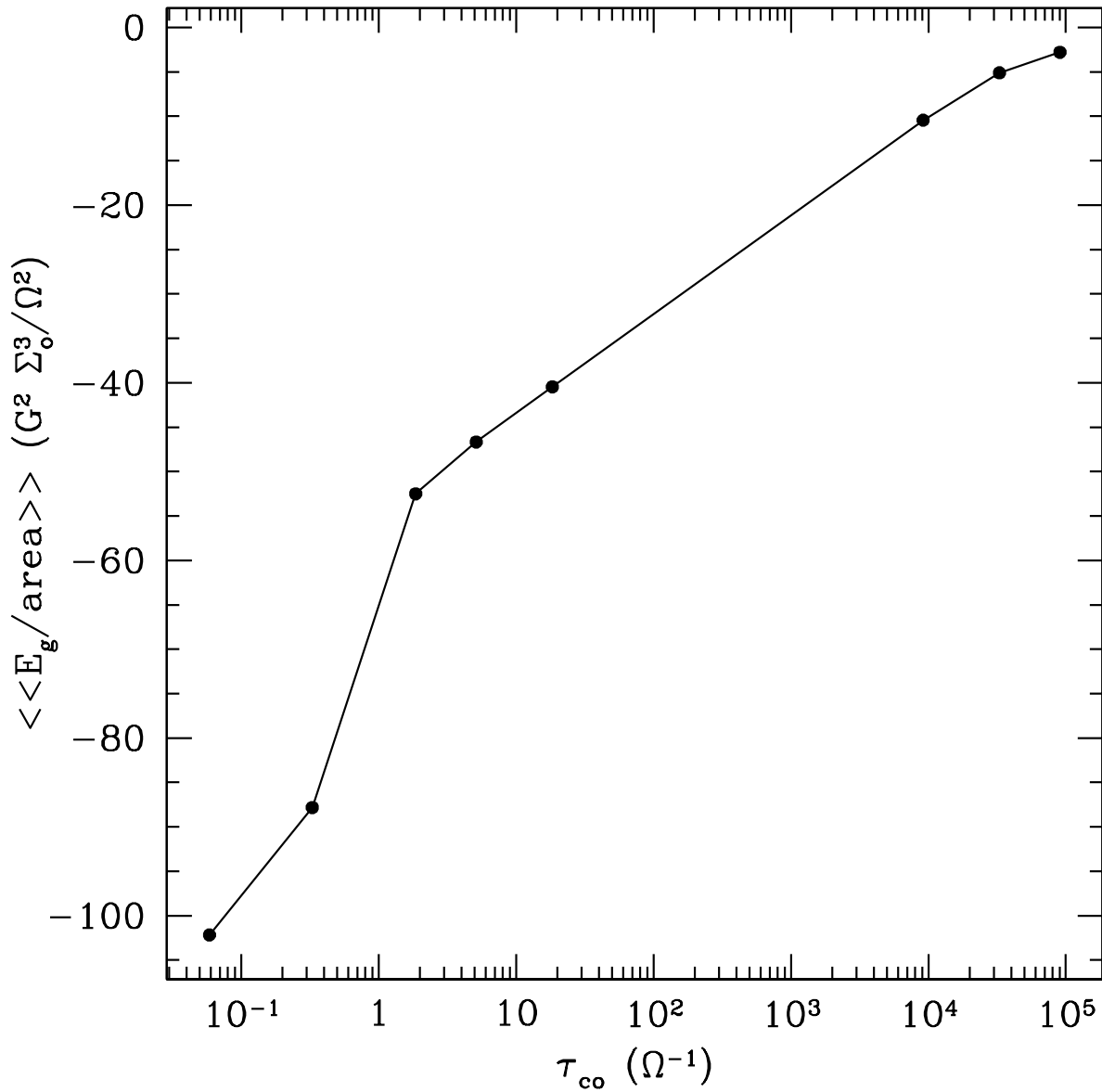


Fig. 8.— Mean gravitational potential energy as a function of initial cooling time for a series of models with varying initial cooling time and $T_o = 1200$.

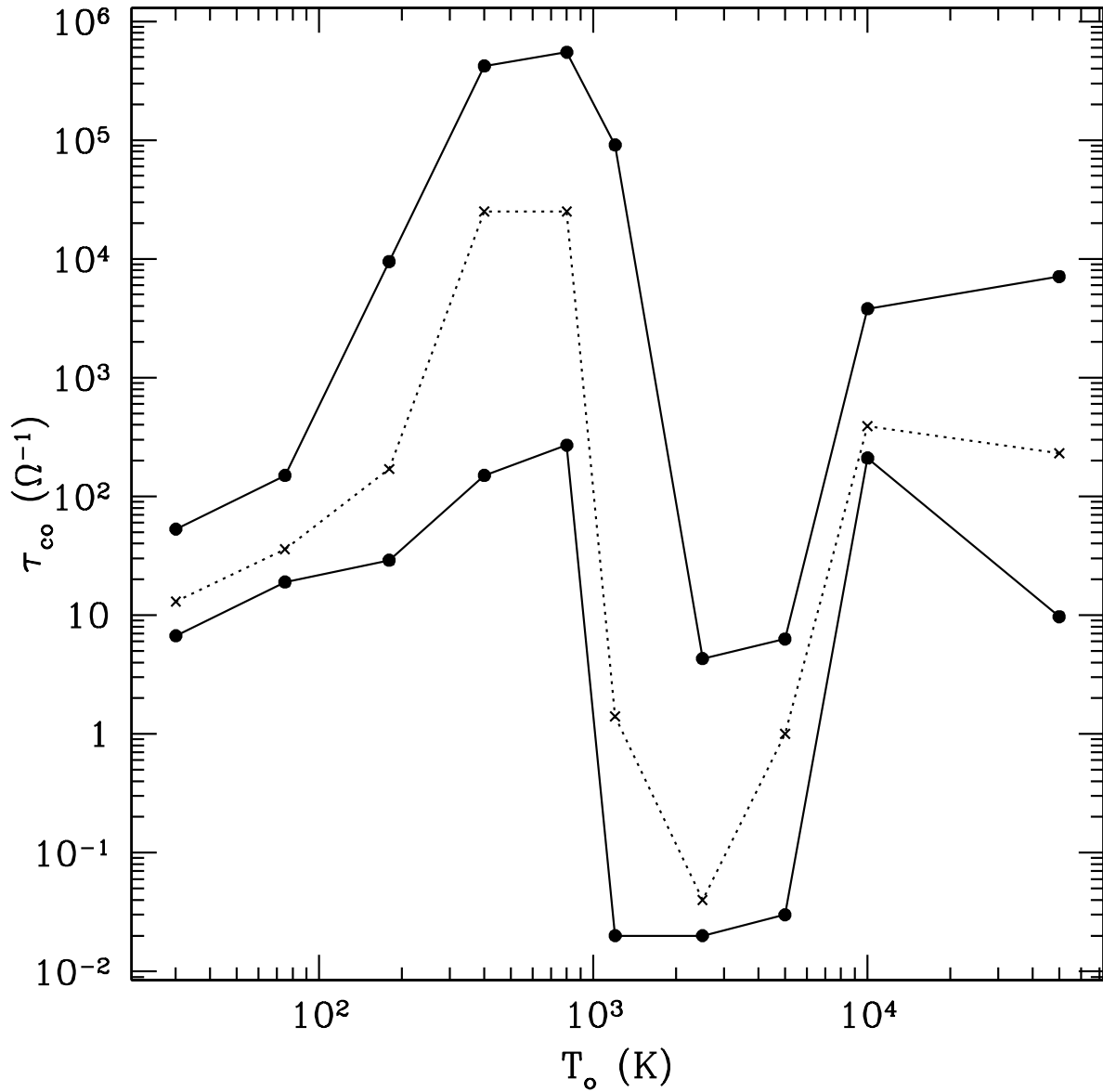


Fig. 9.— Initial cooling times at the points of non-fragmentation, fragmentation and transition.

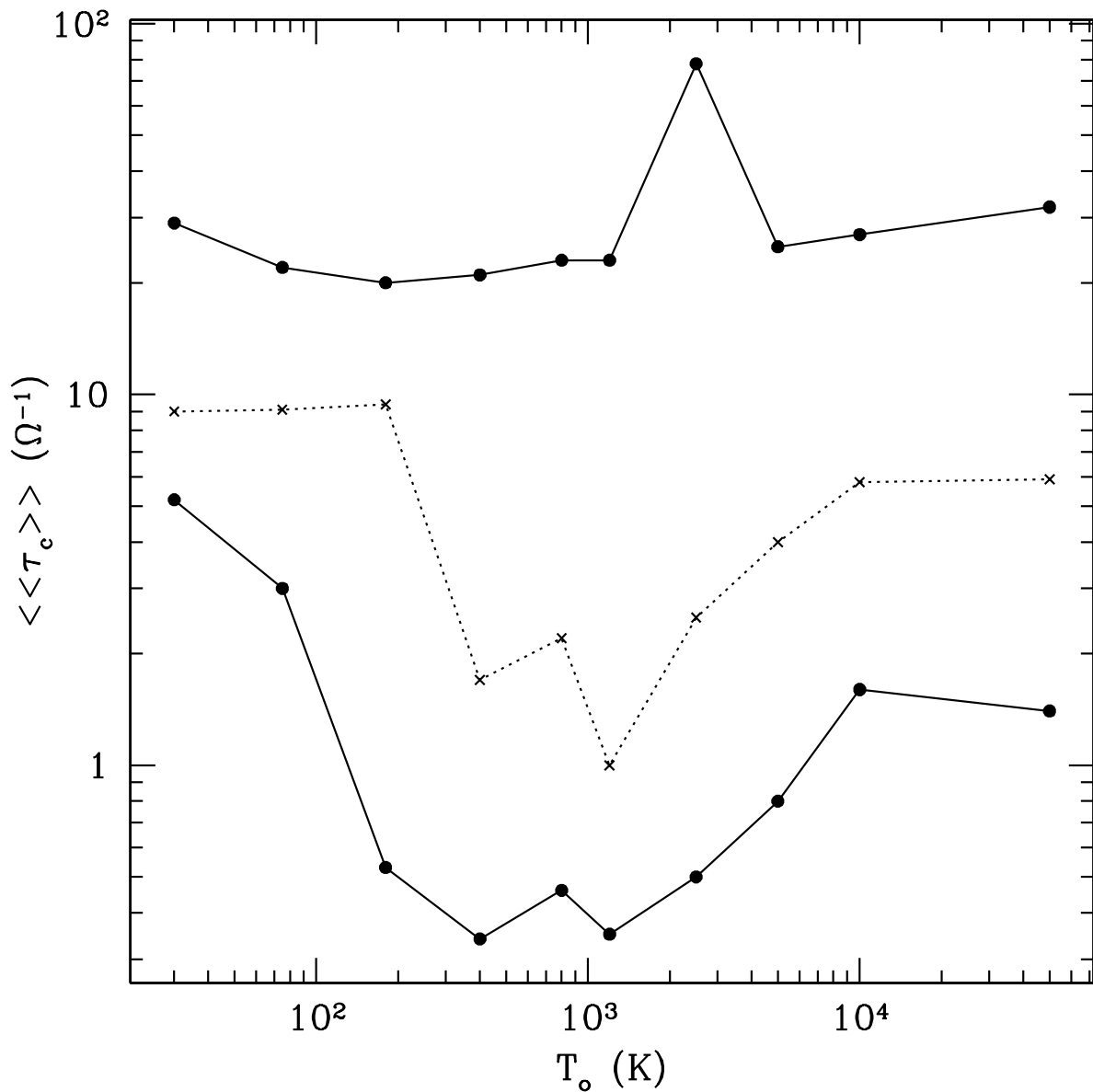


Fig. 10.— Effective cooling times at the points of non-fragmentation, fragmentation and transition.

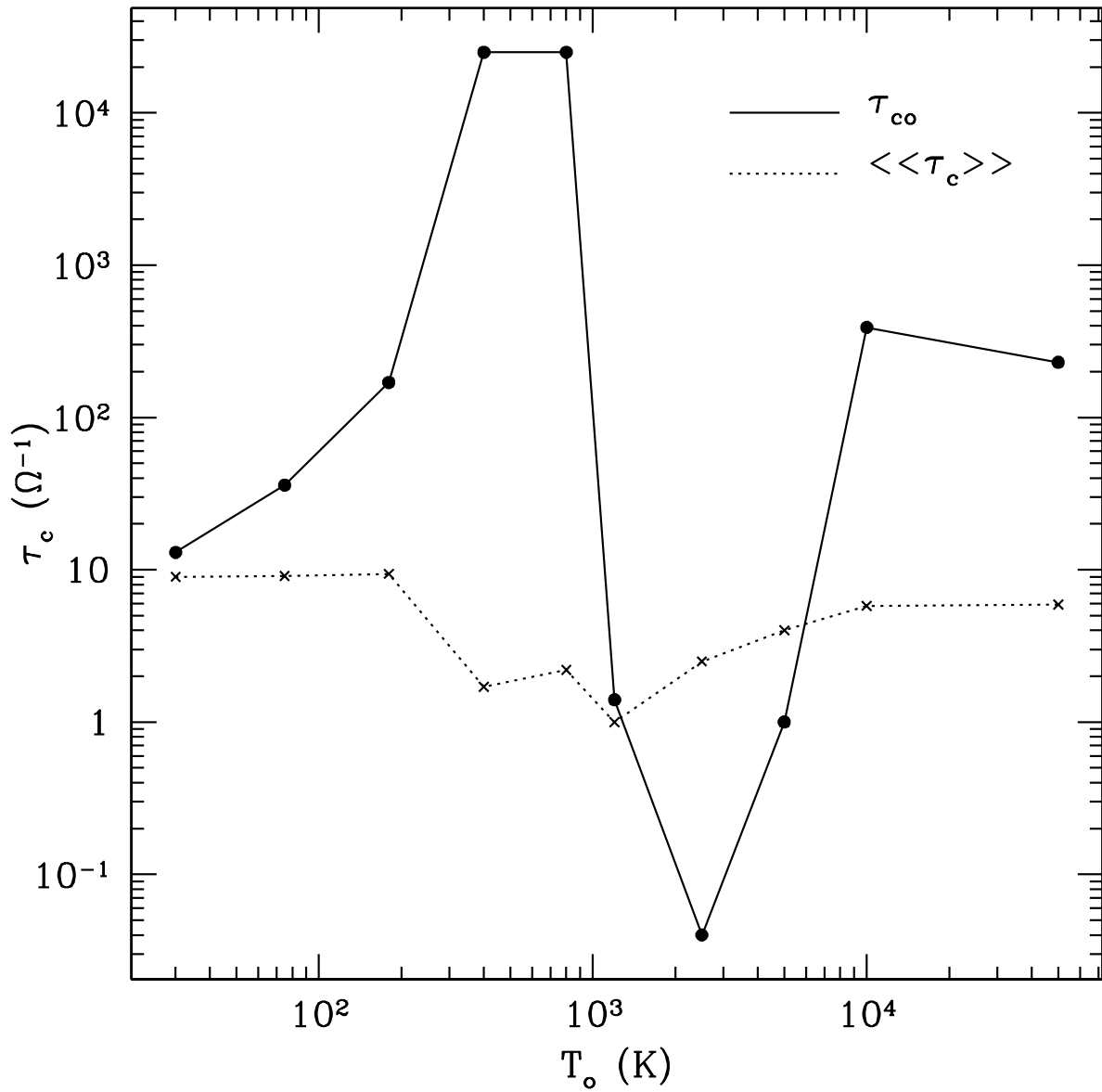


Fig. 11.— Initial and effective cooling times at the transition between non-fragmentation and fragmentation.

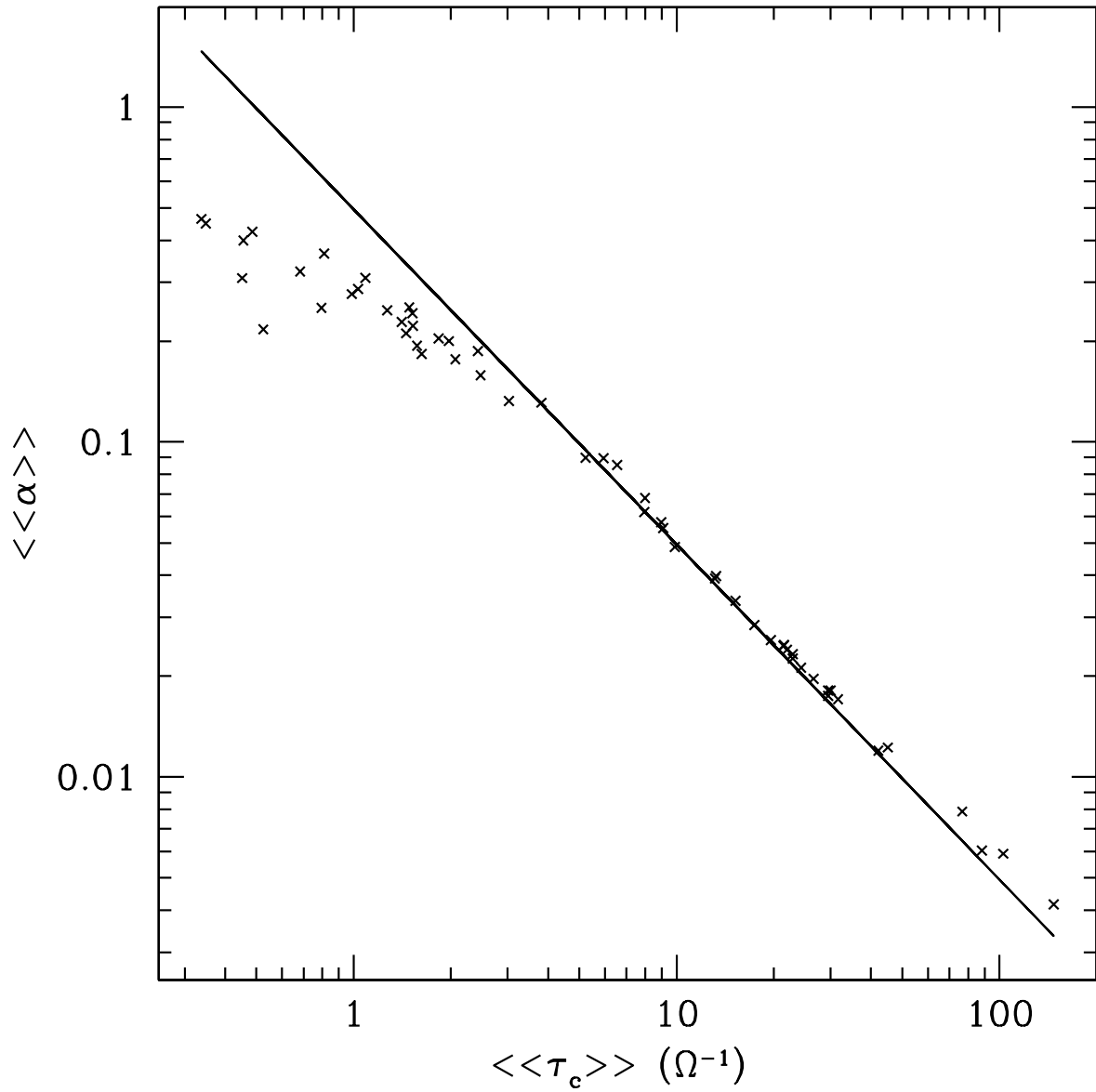


Fig. 12.— Time-averaged shear stress vs. effective cooling time for a series of runs. The solid line shows the analytic result, based on energy conservation, from equation (25).